Ponderomotive bunching of a relativistic electron beam for a superradiant Thomson source

B. H. Schaap [1,*] C. W. Sweers,[1] P. W. Smorenburg,[2] and O. J. Luiten[1]

[1]*Department of Applied Physics, Eindhoven University of Technology, P.O. Box 513, 5600 MB Eindhoven, The Netherlands*

[2]*ASML, Netherlands B.V., P.O. Box 324, 5500 AH Veldhoven, The Netherlands*

(Received 25 January 2023; accepted 30 June 2023; published 31 July 2023)

Imposing a density modulation on an electron beam may improve the brightness of a Thomson source by orders of magnitude via superradiant emission. In this paper, we analytically and numerically analyze electron beam modulation via the ponderomotive force due to the copropagating beat wave formed by two laser pulses at different frequencies. We show that energy modulation favorably scales with electron beam energy but is limited by the interaction length imposed by the finite waist of the laser pulses. Additionally, the effect of initial emittance and energy spread on the quality of microbunching is studied. Finally, we propose a superradiant extreme ultraviolet Thomson source based on ponderomotive bunching.

DOI: 10.1103/PhysRevAccelBeams.26.074401

I. INTRODUCTION

Compact sources offering high-brightness radiation in the extreme ultraviolet to x-ray regime are highly desired. An upcoming approach is Thomson scattering, also referred to as inverse Compton scattering, in which a relativistic electron beam colliding with a laser pulse generates radiation [1–5]. The short wavelength of the laser pulse allows for significantly more compact accelerator setups than alternative sources such as synchrotrons and free electron lasers, providing widespread availability and increasing the number of potential applications. Furthermore, by imposing a density modulation on the electron beam, the intensity of the Thomson source can be enhanced via superradiant emission, by orders of magnitude [6,7]. Realizing a superradiant Thomson source would have a tremendous societal impact. However, the microbunching of electrons with the beam energy relevant to Thomson sources is a challenge that has yet to be met.

Several compact prebunching methods have been proposed. For instance, transverse modulation, attained by masking or diffraction on a crystalline solid, is converted to a longitudinal modulation by transportation through an emittance exchange (EEX) line [6–8]. Microbunches can also be generated at the source by photoemission from shaped laser pulses [9] or periodically modulated ionization of a laser-cooled gas [10,11]. Another method is to impart an energy modulation that converts into a density modulation by velocity bunching. The modulation can be realized by time-varying electric fields [12–14] or the inverse FEL process [15].

Another approach to impose an energy modulation is via the ponderomotive force from two lasers at different frequencies [16]. As illustrated schematically in Fig. 1, the two lasers have different propagation axes with respect to the electron beam axis such that the group velocity of the ponderomotive beat wave v_{pond} is matched to the electron beam velocity v_e. The longitudinal phase space dynamics of the center part of the electron beam for a single period of the beat wave is illustrated in Figs. 1(a)–1(c). Before interaction [Fig. 1(a)], the electron beam has a uniform density with an rms energy spread of $\sigma_\gamma m_e c^2$, where $\gamma = (1 - v_e^2/c^2)^{-1/2}$ is the average Lorentz factor of the electron beam, m_e the mass of an electron, and c the speed of light. Subsequently, in the overlap region with the two laser pulses [Fig. 1(b)], the ponderomotive beat wave imposes a sinusoidal energy modulation with amplitude $\Delta\gamma m_e c^2$. Finally, after a drift length $L = f$ [Fig. 1(c)], the higher energy part of the electron beam overtakes the low energy part, leading to a peaked density distribution. The width of the peak, approximately given by $\lambda_b = \sigma_\gamma \lambda_{\mathrm{mod}}/(2\pi\Delta\gamma)$, where $\lambda_{\mathrm{mod}} = 2\pi v_e/(\omega_2 - \omega_1)$ the modulation wavelength with ω_j the angular frequency of the jth laser pulses, determines the shortest wavelength at which superradiance can still occur.

By this method, several keV of energy modulation amplitude has been applied with sub-milliJoule laser pulses, resulting in electron bunches as short as $\lambda_b \simeq 26$ nm [17]. However, these experiments were carried out using an ultralow emittance electron microscopy source with less

*b.h.schaap@tue.nl

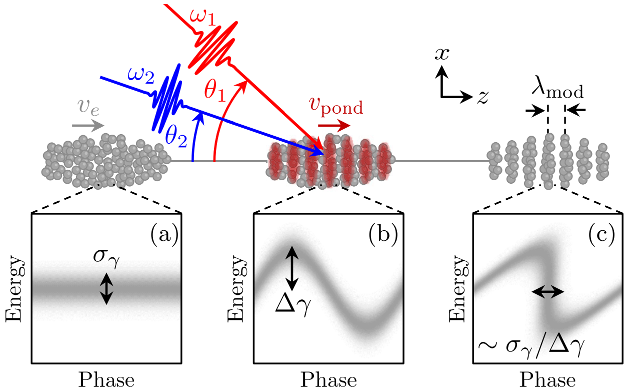

FIG. 1. Schematic of ponderomotive bunching. (a)–(c) Longitudinal phase space distribution along a bunching period.

than a single electron per pulse. For sufficient superradiant emission, the density modulated electron bunch should consist of abundant charge on the picocoulomb level preferably at tens of MeV of beam energy [18]. Moreover, the emittance and energy spread of such highly charged bunches usually are orders of magnitude larger than that of a typical electron beam in an electron microscope.

Nonetheless, in this paper, we present a theoretically and numerically study showing that ponderomotive bunching is suitable for a compact superradiant Thomson source. First, in Sec. II, we treat the basic theory of ponderomotive bunching using a plane wave model. We find expressions for the relevant energy modulation parameters and calculate the bunching quality. Then in Sec. III, we add a finite energy spread and angular spread of the electrons to the model and analyze the resulting bunching factor. In Sec. IV, the effect of a finite extent of the laser pulse and electron beam on bunching is studied. In Sec. V, we end with a concrete proposal for a superradiant Thomson source based on a ponderomotive buncher.

II. BASIC THEORY OF PONDEROMOTVE BUNCHING

A. Energy modulation

Here we treat the basic properties of ponderomotive bunching with covariant electrodynamics, using the metric $g^{\mu\nu} = \mathrm{diag}(1,-1,-1,-1)$. Since some of these properties are already discussed in [16], we aim to cover them concisely. To start, let us assume that the vector potential of both laser pulses can be written as a plane wave with constant amplitude such that the superposed normalized vector potential is given by

$$A^\mu = (A_1 \cos\varphi_1 + A_2 \cos\varphi_2)\epsilon^\mu, \tag{1}$$

where $A_j = eE_{0,j}/(mc\omega_j)$ the normalized vector potential amplitude with $E_{0,j}$ the electric field strength ω_j the angular frequency of the jth laser pulse and e the elementary charge. The phase $\varphi_j = k_j^\nu x_\nu$ is determined by four-wave vector $k_j^\nu = \omega_j/c(1, -\sin\theta_j \mathbf{e}_x + \cos\theta_j \mathbf{e}_z)$ with θ_j the angle with respect to the propagation axis of the electron beam, see Fig. 1. The polarization four-vector is given by $\epsilon^\mu = (0, \mathbf{e}_y)$. The beat wave formed by the two lasers is composed of sum and difference frequencies corresponding to, respectively, super- and subluminal phase velocities.

Time averaging the Lorentz force over the fast time scales, see Appendix A, for initial four-velocity $u_0^\nu = \gamma(1, \beta\mathbf{e}_z)$ normal to the polarization four-vector results in the following equation of motion for the four-velocity of the guiding center motion:

$$\partial_{c\tau}\bar{u}^\mu = -\frac{1}{2}\partial^\mu\langle A^\nu A_\nu\rangle, \tag{2}$$

where τ is the proper time and

$$\langle A^\nu A_\nu\rangle = -\frac{1}{2}A_1^2 - \frac{1}{2}A_2^2 - A_1A_2\cos\varphi_- \tag{3}$$

the ponderomotive potential of the beat wave with $\varphi_- = k_-^\nu x_\nu$ the beat wave phase and $k_-^\mu = k_1^\mu - k_2^\mu$ the four-wavevector of the beat wave.

To estimate the energy gained by the electron after interacting for a proper time τ_0 with the beat wave, we integrate Eq. (2) while applying the impulsive approximation $x^\mu \simeq u_0^\mu c\tau + x_0^\mu$ (see conditions in Appendix B). This results in a change of four-velocity equal to

$$\Delta u^\mu = \frac{1}{2}A_1A_2c\tau_0 \sin\varphi_0 \mathrm{sinc}\left(\frac{1}{2}k_-^\nu u_{0\nu}c\tau_0\right)k_-^\mu, \tag{4}$$

where $\varphi_0 = k_-^\nu x_{0\nu}$ the phase with respect to the beat wave at $\tau = 0$ and $\mathrm{sinc}(x) = \sin(x)/x$. This expression describes sinusoidal modulation in momentum and energy at frequency $\omega_1 - \omega_2$. The amplitude of modulation is maximized when the electron beam is on-resonance, i.e., $k_-^\nu u_{0\nu} = 0$, which can be explained intuitively in both the electron beam rest frame and in the lab frame. In the former frame, the condition states that the laser frequencies are equal so that they form a standing wave. In the lab frame, it states that the phase velocity of the subluminal part of the beat wave is matched to the velocity of the electron beam [16]. Furthermore, for purely longitudinal momentum modulation $\Delta u^{1,2} = 0$, we find the additional condition $k_-^{1,2} = 0$. By combining the resonance condition and the longitudinal modulation condition, we find an expression for angle θ_j as a function of the laser frequencies and resonant electron beam energy:

$$\cos\theta_1 = \frac{1}{\beta}\left(1 - \frac{1}{2\gamma^2}\frac{\omega_1 + \omega_2}{\omega_1}\right). \tag{5}$$

The angle θ_2 can be found by changing the subscripts in (5) from $1 \to 2$ and vice versa. Note that the ponderomotive bunching method also allows for the generation of tilted microbunches. Under certain conditions, such microbunches are relevant to superradiant Thomson scattering [18]. The application of tilted momentum modulation, however, changes the conditions for the laser beam angles. A brief discussion on tilted microbunching is given in Appendix C.

Now suppose that the interaction time is N_0 periods of laser 1 so that $\tau_0 = 2\pi N_0/(ck_1^\nu u_{0\nu})$. Since the proper velocity u_0^μ scales with γ, one would expect that the proper interaction time and thus the energy modulation scales with $\tau_0 \sim 1/\gamma$. However, for higher beam energies, the laser angles θ_j becomes small using a fixed pair of laser frequencies, which effectively increases the interaction length. Substituting the laser angle Eq. (5) into τ_0 gives an interaction time of $\tau_0 = 4\pi N_0\gamma/(\omega_1 + \omega_2)$, which is the same for N_0 periods of laser 2. Therefore, the energy modulation of an on-resonance electron beam also scales favorably with beam energy. By plugging the interaction time into the $\mu = 0$ component of Eq. (4), one finds the energy modulation amplitude given by

$$\Delta\gamma = 2\pi\gamma A_1 A_2 N_0 \frac{\omega_1 - \omega_2}{\omega_1 + \omega_2}, \tag{6}$$

such that the energy modulation is given by $\Delta\gamma \sin\varphi_0$. In reality, the number of interaction periods N_0 is limited by the finite spatiotemporal extent of the laser pulses, which will be addressed in later Sec. IV. The scaling with beam energy allows for strong energy modulation of a 4.6-MeV beam ($\gamma = 10$) at a few to tens of MeV electron beam energy. For example, the energy modulation amplitude induced by a laser pulse with $N_0 = 100$ cycles at $\omega_1 = 2.4 \times 10^{15}$ rad/s ($\lambda_1 = 800$ nm) and a laser pulse at the third harmonic $\omega_2 = 3\omega_1$, both having a normalized vector potential of $A_1 = A_2 = 0.002$ is about 6.4 keV. We will use this set of nominal parameters to illustrate the following important quantities.

B. Microbunch formation

Following energy modulation, electrons with higher energy will start to overtake the lower energy part of the beam, leading to longitudinal foci along the beam axis, where the electron density is significantly increased as illustrated in Fig. 1. The focal length f, after which the beam energy modulation has fully converted into a density modulation, can be found by expanding the phase after a drift L given by $\varphi = \varphi_0 + L\Delta\beta/\beta \sin\varphi_0$ with $\Delta\beta \simeq \Delta\gamma/(\gamma^3\beta)$, the change in normalized velocity due to the energy modulation, around $\varphi_0 = \pi$. The drift length for this case at which the phase becomes zero corresponds to the focal length given by

$$f = \frac{c\gamma^2\beta^3}{2\pi A_1 A_2 N_0} \frac{\omega_1 + \omega_2}{(\omega_1 - \omega_2)^2}. \tag{7}$$

Even for electron beam energies of few to tens of MeV, generic to Thomson sources, the focal length can be quite short and does not require beam line elements that increase the dispersion. For example, for the nominal parameters in the previous section, the focal length is $f = 5$ mm.

Next, the microbunching quality is quantified by calculating the Fourier component b_n at frequency nck_-^0, with n an integer, of the resulting density distribution along the beat wave period at the center of the bunch. The Fourier component b_n, also known as the bunching factor, is an important figure of merit for superradiance. It directly quantifies the amplification factor of the power in superradiant Thomson scattering

$$P_{\mathrm{SR}} = \frac{\pi}{4}\chi\alpha A_0^2 N_L P_{\mathrm{ebeam}} \frac{|b_n|^2 N_e}{nN_b}\eta, \tag{8}$$

where recoil parameter $\chi = \hbar\omega_X/(\gamma m_e c^2)$ is the ratio between the energy of an emitted photon $\hbar\omega_X$ and the electron energy, α the fine-structure constant, A_0 the normalized laser vector potential, N_L the number of laser periods, N_b the number of microbunches and $P_{\mathrm{ebeam}} = N_e\gamma m_e c^2 f_{\mathrm{rep}}$ the average electric power, with N_e the number of electrons and f_{rep} the repetition rate. Note that in Eq. (8), the transverse size of the electron beam has not been taken into account, which can lead to a significant reduction of superradiant power [18].

For now, we will assume that the initial density distribution of the electron beam is uniform $n_e(\varphi_0) = n_{e,0}$ with $n_{e,0}$ the number of electrons per beat wave period and that all electrons are on-resonance. The density distribution after modulation can be written as the following Fourier series $n_e(\varphi) = n_{e,0}\sum_{n=1}^{\infty} b_n \exp(in\varphi_0)$, where the Fourier coefficients given by $b_n = 1/(2\pi n_{e,0})\int_0^{2\pi} d\varphi n_e(\varphi)\exp[-in\varphi]$ correspond to the bunching factor given in Eq. (8). Since the distribution function is conserved along its trajectories, we can write the integrand in this case as $n_e(\varphi)d\varphi = n_{e,0}d\varphi_0$. Next, we substitute $\varphi = \varphi_0 + \zeta\sin\varphi_0$, where $\zeta = L/f$, into the expression for the Fourier components b_n, which after integrating results in

$$b_n = (-1)^n J_n(n\zeta), \tag{9}$$

where $J_n(x)$ is the nth-order Bessel function of the first kind. The expression gives the best case bunching factor or the nth harmonic of the modulation frequency using this method without any other effects, such as finite energy spread, taken into account. For high harmonics $n \geq 4$, its maximum $\max[J_n(x)] \simeq 0.67n^{-1/3}$ occurs when the argument is $x \simeq n + 0.81n^{1/3}$ corresponding to a drift length of $\zeta = 1 + 0.81n^{-2/3}$. Assuming optimized bunching at the tenth harmonic $b_{10} \simeq 0.311$ of a 5-pC electron bunch, with $N_b = 100$ microbunches, results in an amplification factor of

$|b_{10}|^2 N_e = 3 \times 10^6$ in 0.1% bandwidth with respect to the incoherent case.

III. ENERGY SPREAD AND ANGULAR SPREAD

In the previous section, it was assumed that each electron is perfectly on-resonance. In reality, however, an electron beam has a finite energy spread σ_γ and a finite transverse angular spread σ_θ. Off-resonant electrons are therefore inevitable, affecting the microbunching process in the following two ways: First, during interaction, off-resonant electrons will probe different phases of the ponderomotive wave, resulting in a lower average energy modulation and an additional spread in energy modulation on top of the initial energy spread. Second, after energy modulation, off-resonant electrons result in a spread of arrival time at the longitudinal focus, leading to a larger microbunch width. Here, we will quantify these effects for energy spread and angular spread separately.

A. Energy spread

An electron with an off-resonant energy described by four-velocity $u_0^\mu = (\gamma + \delta\gamma)(1, [\beta + \delta\gamma/(\gamma^3\beta)]\mathbf{e}_z)$, where $\delta\gamma = \gamma' - \gamma$ the deviation from the on-resonance Lorentz factor γ, propagates at a different velocity than the beat wave phase velocity formed by the two laser pulses. The rate at which the phase of the electron changes with respect to the beat wave follows from $k_-^\nu u_{0\nu} = \delta\gamma(1 + \delta\gamma/\gamma)(\omega_1 - \omega_2)/(c\beta^2\gamma^2)$. First, the effect of off-resonant electrons on the energy modulation process will be studied. Then, we quantify how it influences the subsequent density modulation process. We consider an electron beam with an initial Gaussian energy distribution $f_0 = 1/(\sqrt{2\pi}\sigma_\gamma)\exp[-\delta\gamma^2/(2\sigma_\gamma^2)]$, with σ_γ the rms normalized energy spread as illustrated in Fig. 1(a).

The average energy modulation is analytically calculated by substituting the expression for $k_-^\nu u_{0\nu}$ above in Eq. (4) and performing a weighted average of the zeroth component $\langle\Delta\gamma\rangle = \int \Delta u^{(0)} f_0 d(\delta\gamma)$. To first order in the relative energy spread σ_γ/γ, we find that

$$\langle\Delta\gamma\rangle = \Delta\gamma \frac{\sqrt{\pi}}{2}\frac{\mathrm{erf}\xi}{\xi}, \tag{10}$$

where $\xi = \sqrt{\pi}\sigma_\gamma N_0(\omega_1 - \omega_2)/[\gamma\beta^2(\omega_1 + \omega_2)]$, which is a measure for the rms phase change during energy modulation, and $\mathrm{erf}(x) = (2/\sqrt{\pi})\int_0^x \exp(-y^2)dy$ is the error function. The beam energy spread, as expected, decreases the mean energy modulation, which is clearly shown by the Taylor series at $\xi = 0$ given by $\langle\Delta\gamma\rangle \simeq \Delta\gamma(1 - \xi^2/3)$. However, if the rms phase change is much less than one beat wave cycle such that $\xi \ll 1$, the energy modulation can be described by Eq. (6), which is the case for the nominal set of parameters with an initial energy spread of 1 keV ($\xi = 0.019$).

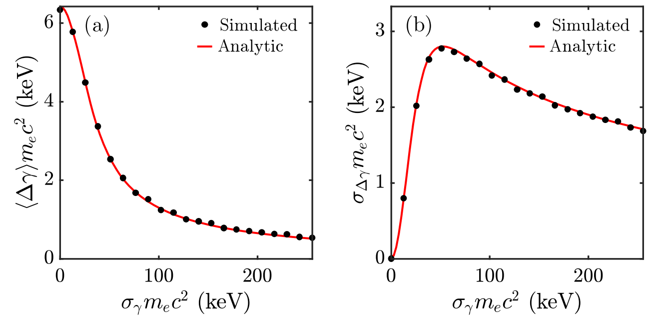

FIG. 2. (a) Average energy modulation and (b) spread in energy modulation due to electron beam energy spread.

In Fig. 2(a) the average energy modulation amplitude due to energy spread given by Eq. (10) is plotted for the nominal set. The analytically calculated curves match the results from particle tracking simulations (black dots) using General Particle Tracer (GPT) [19], which integrates the equations of motion of the electrons in the electromagnetic fields without approximations. Note that in this work, we do not take into account Coulomb forces in the particle tracking simulations. For the nominal set, the average energy modulation only decreases significantly for a beam energy spread much larger than the energy modulation. Such high energy spread with respect to the energy modulation, as will be discussed later on, is highly impractical for the formation of microbunching.

Similarly, the beam energy spread induced by the interaction leads to an additional spread in energy modulation. The rms energy modulation is given by $\sigma_{\Delta\gamma} = (\langle\Delta\gamma^2\rangle - \langle\Delta\gamma\rangle^2)^{1/2}$, where the second moment is $\langle\Delta\gamma^2\rangle = \int \Delta u^{(0)2} f_0 d(\delta\gamma)$. Using Eqs. (4) and (10), we obtain

$$\sigma_{\Delta\gamma} = \frac{\Delta\gamma}{2\xi}[\exp(-4\xi^2) - 1 - \pi\mathrm{erf}(\xi)^2 + 2\sqrt{\pi}\xi\mathrm{erf}(2\xi)]^{1/2}. \tag{11}$$

For small ξ, the rms spread in energy modulation is given by $\sigma_{\Delta\gamma} \simeq \sqrt{2}\Delta\gamma\xi^2/3$. The total energy spread after modulation is approximately given by $(\sigma_\gamma^2 + \sigma_{\Delta\gamma}^2)^{1/2}$. The energy spread is thus only increased significantly when the spread in energy modulation becomes larger than the initial beam energy spread.

For the nominal set, as shown in Fig. 2(b), the spread in energy modulation does not become larger than the initial spread, which holds in most practical cases. Therefore, this effect is rather unimportant. Furthermore, bunching becomes highly impractical if the initial energy spread is larger than the energy modulation amplitude.

However, the initial energy spread does significantly affect the microbunching formation. Assuming that the energy modulation is unaffected by the energy spread, $\xi \ll 1$, we can write the phase advance of the electron after modulation as follows $\varphi = \varphi_0 + \zeta\delta\gamma/\Delta\gamma + \zeta \sin\varphi_0$, where the second term gives the extra phase slip due to the off-resonant energy. Note that we again neglected the second order term in the relative energy spread. Using the same method as in Sec. II B including the initial energy distribution f_0 and taking into account the additional off-resonant term in the phase advance, the bunching factor $b_n = 1/(2\pi)\int_0^{2\pi} d\varphi_0 \int_{-\infty}^{\infty} f_0 \exp[-in\varphi] d(\delta\gamma)$ can be calculated. Evaluating the integral results in

$$b_n = (-1)^n J_n(n\zeta) \exp\left[-\frac{1}{2} n^2 \zeta^2 \frac{\sigma_\gamma^2}{\Delta\gamma^2}\right], \tag{12}$$

which is the well-known expression for the bunching factor in high gain high harmonic generation [20]. The exponential term resulting from finite energy spread suppresses the maximum bunching factor without energy spread given by the Bessel function. Physically, this is caused by the smallest attainable bunch width λ_b as shown in Fig. 1(c) due to the varying arrival times. If the energy modulation is impacted by the initial energy spread, then in good approximation, one can substitute $\zeta \to \zeta\Delta\gamma/\langle\Delta\gamma\rangle$ and $\sigma_\gamma \to (\sigma_\gamma^2 + \sigma_{\Delta\gamma}^2)^{-1/2}$ in Eq. (12).

The analytic bunching factor for a beam energy spread of 0.46 keV of the fundamental and fourth harmonic agree with the GPT simulations, as is depicted in Fig. 3. Such beam energy spreads are reached using conventional photoguns generating electron bunches with a charge of 100 fC [21,22] or bunches with several pC using a modern thermionic gun concept [23]. The bunching factor of the fundamental is hardly impacted by the beam energy spread with respect to the bunching factor of a monoenergetic beam given by the dashed solid curve. However, the maximum of the higher harmonic order is reduced by about 10% in the absolute bunching factor.

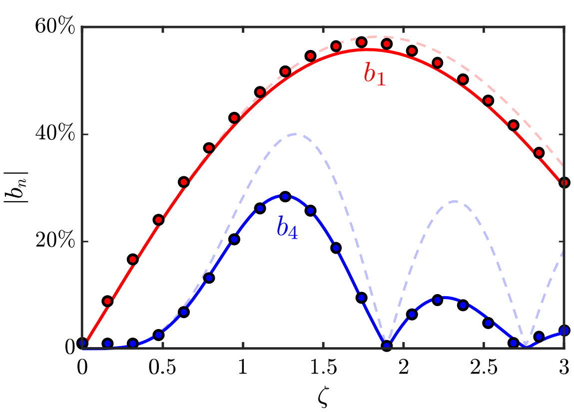

FIG. 3. Simulated (dots) and analytically calculated (solid curves) bunching factor of the fundamental and fourth harmonic with energy spread $\sigma_\gamma = 10^{-3}$. Analytically calculated bunching factor without energy spread is given by the dashed curve.

B. Angular spread

To calculate the effect of the angular spread on energy modulation and bunching, we consider an electron with four-velocity $u_0^\mu = \gamma(1, \beta\theta_x \mathbf{e}_x + \beta\theta_y \mathbf{e}_y + \beta[1 - (\theta_x^2 + \theta_y^2)/2]\mathbf{e}_z)$, where θ_x and θ_y are small angles the electron makes in the xz and yz plane, respectively. The finite angles introduce small perturbations from resonance, such that $k_-^\nu u_{0\nu} = (\theta_x^2 + \theta_y^2)(\omega_1 - \omega_2)/(2c)$. In the following, a Gaussian angular distribution described by the distribution function $f_0 = 1/(2\pi\sigma_\theta)\exp[-(\theta_x^2 + \theta_y^2)/(2\sigma_\theta^2)]$ is assumed, where σ_θ is the rms angular spread.

First, the average energy modulation is calculated assuming that the angular spread only affects the electron resonance. Taking the weighted average $\langle\Delta\gamma\rangle = \int \Delta u^{(0)} f_0 d\theta_x d\theta_y$, where $u^{(0)}$ is evaluated at phase $\varphi_0 = \pi/2$, results in the following average energy modulation amplitude

$$\langle\Delta\gamma\rangle = \Delta\gamma \frac{\arctan(\chi)}{\chi}, \tag{13}$$

where $\chi = \gamma^2\sigma_\theta^2 2\pi N_0(\omega_1 - \omega_2)/(\omega_1 + \omega_2)$ is a measure for the accumulated phase change after the interaction. For small χ, the average energy modulation is given by $\langle\Delta\gamma\rangle \simeq \Delta\gamma(1 - \chi^2/3)$. At $\chi = 0$, the energy modulation is equal to the cold beam modulation. When $\chi = 2.3$, the energy modulation is suppressed by the angular spread by a factor of 2.

In Fig. 4(a), the drop of average energy modulation amplitude due to angular spread given by Eq. (13) is plotted for the nominal set. At an angular spread of 10 mrad, the average energy modulation amplitude is about half the optimal energy modulation amplitude. Assuming an electron beam waist of $\sigma_r = 5$ μm, the normalized transverse emittance $\epsilon_n = \gamma\beta\sigma_\theta\sigma_r$ of the electron beam corresponding to the angular spread at this point is $\epsilon_n = 500$ nm rad. This is much larger than the emittance of electron bunches from photoinjectors with a charge of tens of pC [24,25].

The spread in energy modulation due to angular spread can be calculated using the second moment $\langle\Delta\gamma^2\rangle = \int \Delta u^{(0)2} f_0 d\theta_x d\theta_y$, resulting in

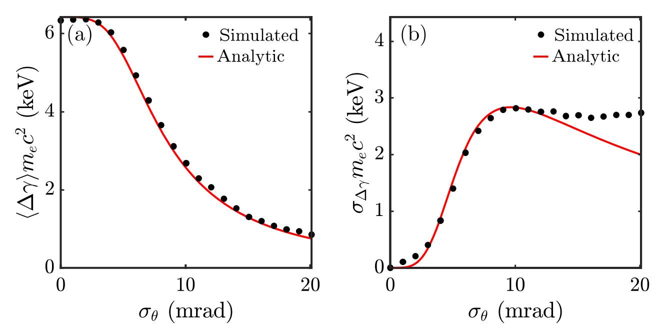

FIG. 4. (a) Average energy modulation and (b) spread in energy modulation due to electron beam angular spread.

$$\sigma_{\Delta\gamma} = \frac{\Delta\gamma}{2\chi}\{4\chi\arctan(2\chi) - \arctan^2(\chi) - \ln(1+4\chi^2)\}^{1/2}. \quad (14)$$

The spread in energy modulation increases with the rms phase change, as becomes clear from the Taylor expansion around $\chi = 0$ given by $\sigma_{\Delta\gamma} \simeq \sqrt{5}\Delta\gamma\chi^2/3$.

In Fig. 4(b), the average spread in energy modulation due to angular spread given is plotted for the nominal set. For low angular spread, the spread in energy modulation steadily increases until it almost reaches 3 keV around 8 mrad. Then, the spread in energy modulation decreases as a result of even stronger dephasing combined with a significantly lower average modulation amplitude. Note that in this regime, the analytic results do not match the simulation very well. The additional spread in energy modulation in the simulation is not induced by the ponderomotive force, however, but is rather an artifact of the initialization of the electron in the plane wave.

The dominant effect of finite angular spread, however, is that a curved density modulation will form after a certain drift length as is depicted in the inset figure in Fig. 5. Assuming that the energy modulation is unaffected by the angular spread, we can write the phase advance of the electron after modulation as follows $\varphi = \varphi_0 + \zeta\gamma^3\beta^2(\theta_x^2+\theta_y^2)/(2\Delta\gamma) + \zeta\sin\varphi_0$, where the second term gives the extra phase slip due to the finite initial angle. Evaluating the integral $b_n = 1/(2\pi)\int_0^{2\pi} d\varphi_0 \int_{-\infty}^{\infty}\int_{-\infty}^{\infty} f_0 \exp[-in\varphi]d\theta_x d\theta_y$ results in the following bunching factor

$$b_n = (-1)^n J_n(n\zeta)\frac{\exp\left[-i\arctan\left(n\zeta\frac{\gamma^3\beta^2\sigma_\theta^2}{\Delta\gamma}\right)\right]}{\sqrt{1+n^2\zeta^2\frac{\gamma^6\beta^4\sigma_\theta^4}{\Delta\gamma^2}}}. \quad (15)$$

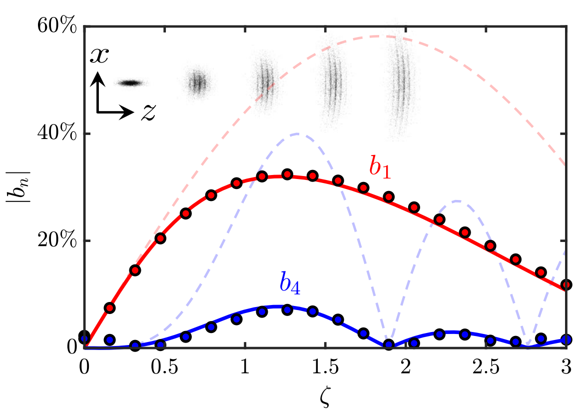

FIG. 5. Simulated (dots) and analytically calculated (solid curves) bunching factor of the fundamental and fourth harmonic with $\sigma_\theta = 2.5$ mrad angular spread. The analytic bunching factor without angular or energy spread is indicated by the dashed curves.

Stronger bunching curvature induces a larger microbunch width when projected on the axis, suppressing the bunching factor significantly, which is quantified by the square root term in Eq. (15). Because the bunching factor maximizes around the $\zeta \simeq 1$, we find that the angular spread should satisfy the condition $\sigma_\theta^2 \ll \Delta\gamma/(n\gamma^3\beta^2)$ to not considerably deteriorate the longitudinal bunching. For the nominal set of parameters with optimized superradiance at the tenth harmonic, (40 nm), the allowable angular spread using this condition is 1.2 mrad. At such angular spread, the induced spread in energy modulation for the nominal set is negligible. Note, however, that this could be taken into account since the curvature is independent of the spread in energy modulation or initial energy spread. The argument of the complex exponent does not influence the superradiant power but adds a constant phase term to the bunching factor.

Figure 5 shows that the analytic bunching factor of the fundamental and fourth harmonic for the nominal set, with an angular spread of 2.5 mrad, are in good agreement with the GPT simulations. Although the energy modulation is hardly impacted by the angular spread, the bunching factor of both orders declines strongly due to the induced curvature. The normalized transverse emittance for this beam, assuming again a waist of 5 μm, is 50 nm rad. Highly charged bunches of several pC at such low emittance can be generated using a modern thermionic injector [23,26].

IV. FINITE SIZE EFFECTS OF THE ELECTRON BEAM AND LASER PULSES

In the previous section, the bunching factor was calculated for a single beat wave period assuming an infinitely long plane wave with infinite transverse extent. However, in reality, both the electron beam and laser beam have a finite transverse and longitudinal extent. The consequence is an inhomogeneous energy modulation of the electron beam. Since the energy modulation determines the focal length, the time at which the local bunching factor at a given part of the beam will be optimized may differ from other parts, leading to a reduced macroscopic bunching factor and superradiance. Here we will first study the effect of a finite laser pulse and electron beam length. Then, we will also take into account the finite transverse sizes of all beams.

A. Finite longitudinal size

Now we assume that the amplitude of both laser pulses is varying along their axes. We consider Gaussian laser pulse envelopes resulting in a normalized four-potential

$$A^\mu = \left[A_1\exp\left(-\frac{\varphi_1^2}{2\sigma_{\varphi_1}^2}\right)\cos\varphi_1 + A_2\exp\left(-\frac{\varphi_2^2}{2\sigma_{\varphi_2}^2}\right)\cos\varphi_2\right]\epsilon^\mu, \quad (16)$$

where σ_φ is the rms pulse length in radians. In general, the number of oscillations of both laser pulses may differ such that $\sigma_{\varphi_1} \neq \sigma_{\varphi_2}$.

Taking the contraction of the four-potential and averaging over the fast time scales leads to the same expression for the ponderomotive potential as Eq. (3) but with amplitudes substituted by the Gaussian envelopes $A_j \to A_j g(\varphi_j)$ with $g(\varphi_j) = \exp[-\varphi_j^2/(2\sigma_{\varphi_j}^2)]$ the envelope function. Substituting the ponderomotive potential into the ponderomotive force [Eq. (2)] and integrating results in the following energy modulation for on-resonance electrons

$$\Delta\gamma = \sqrt{\pi} A_1 A_2 \gamma \sigma_\varphi \frac{\omega_1 - \omega_2}{\omega_1 + \omega_2} \exp\left[-\frac{\varphi_0^2}{2(\sigma_{\varphi_1}^2 + \sigma_{\varphi_2}^2)}\right], \qquad (17)$$

where $\sigma_\varphi = \sqrt{2}\sigma_{\varphi_1}\sigma_{\varphi_2}/(\sigma_{\varphi_1}^2 + \sigma_{\varphi_2}^2)^{1/2}$ and we assumed that the envelope function is slowly varying with respect to the laser wavelength: $|u_{0\nu}\partial^\nu g(\varphi_j)| \ll |k_j^\nu u_{0\nu} g(\varphi_j)|$. The sinusoidal energy modulation $\Delta\gamma(\varphi_0)\sin\varphi_0$ scales linearly with the electron beam energy γ and both the laser pulse amplitudes A_1 and A_2 as in the plane wave case, see Eq. (6), however, the total amplitude is now dependent on initial phase φ_0 of the electron with respect to the beat wave.

Figure 6 shows the simulated longitudinal phase space just after energy modulation for a 4.6-MeV electron beam modulated for the nominal set with $A_1 = A_2 = 0.005$ and $\sigma_\varphi = \sigma_{\varphi_1} = \sigma_{\varphi_2} = 50$ corresponding to a pulse length of 21 and 7 fs, respectively. The amplitude of the sinusoidal modulation is largest at the center of the beam and becomes increasingly smaller going off-center. The analytic expression for the modulation envelope given by Eq. (17) predicts the simulation correctly.

As a result of the phase dependent energy modulation, each period will compress at a slightly different position downstream of the buncher. This breaks the periodicity so the density distribution cannot be expanded in a Fourier series. In this case, the bunching factor is given by the continuous Fourier transform of the spatial distribution function written as $b(\kappa) = \int d\varphi n_e(\varphi)\exp[-i\kappa\varphi]/N_e$, where κ is a continuous variable representing the bunching frequency with respect to the frequency of the beat wave.

Consider an initial Gaussian longitudinal distribution of monoenergetic electrons described by $n_e(\varphi_0) = N_e/(\sqrt{2\pi}\sigma_e)\exp[-\varphi_0^2/(2\sigma_e^2)]$, where σ_e is the length of the electron beam normalized by the wavelength of the beat wave. Using the phase $\varphi = \varphi_0 + \zeta g(\varphi_0)\sin\varphi_0$, we find that the bunching factor at $\kappa = n$ is given by

$$b_n = \frac{(-1)^n}{\sqrt{2\pi}\sigma_e}\int_{-\infty}^{\infty} d\varphi_0 \exp\left(-\frac{\varphi_0^2}{2\sigma_e^2}\right) \times J_n\left[n\zeta\exp\left(-\frac{\varphi_0^2}{2(\sigma_{\varphi_1}^2 + \sigma_{\varphi_2}^2)}\right)\right], \qquad (18)$$

where $\zeta = L/f$ with $f = c\gamma^3\beta^3/[\Delta\gamma(\omega_1 - \omega_2)]$ the focal length of the center of the electron beam, where $\Delta\gamma$ is evaluated at $\varphi_0 = 0$. The electron beam distribution function in this expression weighs the contribution of the local bunching factor, determined by the energy modulation distribution in the argument of the Bessel function, to the macroscopic bunching factor.

Now, we can study the expression for several cases as illustrated in Fig. 7. First, when the electron beam is much smaller than the laser pulses such that $\sigma_e \ll \sigma_\varphi$, all the electrons experience approximately the same amplitude of the laser pulses and the expression simplifies to Eq. (9) as is shown by the dashed curves in Fig. 7 for the fundamental and eighth harmonic.

Second, when the electron bunch is as long as the laser pulse $\sigma_e = \sigma_\varphi$, the bunching is affected due to the finite modulation envelope. In this case, the maximum of the bunching factor is smaller than the plane wave case.

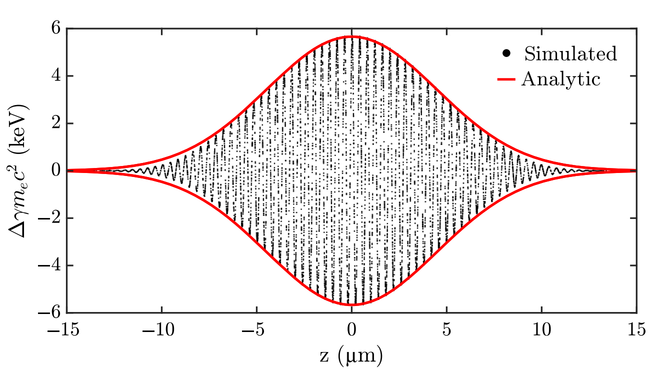

FIG. 6. Analytically calculated energy modulation envelope (red solid curve) corresponds with energy modulation of the GPT simulation (dots) for $A_1 = A_2 = 0.005$ and $\sigma_\varphi = 50$.

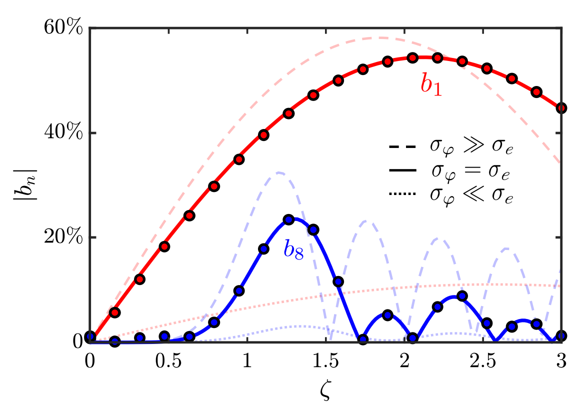

FIG. 7. Simulated (dots) and analytically calculated (continuous curves) bunching factor of the fundamental and eighth harmonic for $\sigma_\varphi = \sigma_e = 50$, with $\sigma_{\varphi_1} = \sigma_{\varphi_2}$ Also, analytic results are shown for $\sigma_\varphi = 50\sigma_e$ (dashed solid curve) and $\sigma_\varphi = 0.1\sigma_e$ (dotted solid curve).

The peak is reached farther downstream than the central focal length since on average there are more electrons off-center that are ideally compressed simultaneously. Consequently, the distance over which there is significant bunching is increased. In this regime, we also performed GPT simulations which are in good agreement with the analytical calculations.

Last, when the laser pulses are much shorter than the electron bunch such that $\sigma_e \gg \sigma_\varphi$, the bunching is influenced by the modulation amplitude and the small fraction of the electron beam that partakes in the modulation. The combination of these two effects significantly lowers the bunching factor as indicated by the dotted solid curves in Fig. 7.

B. Including finite transverse size

Up until now, the laser pulses were modeled as plane waves with infinite transverse extent. However, in reality, both the laser pulses and the electron beam will have a finite transverse waist size, which will affect the bunching process in the following two ways. First, the laser pulse waist will restrict the interaction time significantly, thereby directly limiting the energy modulation. Second, the energy modulation will depend on the transverse electron beam coordinate, leading to different arrival times at the longitudinal focus.

In the following calculations, we will study a laser pulse including a Gaussian transverse profile given by

$$A^\mu \simeq \left[A_1 \exp\left(-\frac{\rho_1^2}{w_{\rho_1}^2} - \frac{\eta^2}{w_{\eta_1}^2} - \frac{\varphi_1^2}{2\sigma_{\varphi_1}^2}\right)\cos\varphi_1 + A_2 \exp\left(-\frac{\rho_2^2}{w_{\rho_2}^2} - \frac{\eta^2}{w_{\eta_2}^2} - \frac{\varphi_2^2}{2\sigma_{\varphi_2}^2}\right)\cos\varphi_2\right]\epsilon^\mu, \quad (19)$$

where $\rho_j = r_j^\nu x_\nu$ and $\eta = \epsilon^\nu x_\nu$ are mutually orthogonal transverse laser coordinates with $r_j^\mu = (0, \cos\theta_j\,\mathbf{e}_x + \sin\theta_j\,\mathbf{e}_z)$ a four-vector denoting the transverse direction of the jth laser pulse. Here, w_{ρ_j} and w_{η_j} are the $1/e$ waist sizes. To satisfy the Lorenz-gauge condition $\partial^\nu A_\nu = 0$ for the above four-potential, there should be a nonzero scalar potential. However, the scalar potential is negligible compared to the vector potential as long as the amplitude is slowly varying with respect to the wavelength of the laser, which we will assume in the following calculations. Note that this expression describes a Gaussian TEM_{00} mode laser beam close to its focus, neglecting beam divergence and the radial and Gouy phase change.

Following the plane wave analysis, see Appendix D, we substitute the ponderomotive potential $\langle A_\nu A^\nu\rangle$ into the ponderomotive force Eq. (2) and integrate it over proper time. This results in the following energy modulation for on-resonance electrons

$$\Delta\gamma = \sqrt{\pi}A_1A_2\gamma\sigma_{3\mathrm{D}}\frac{\omega_1-\omega_2}{\omega_1+\omega_2} \times \exp\left(-\frac{x_0^2}{2\sigma_x^2} - \frac{y_0^2}{2\sigma_y^2} - \frac{z_0^2}{2\sigma_z^2} + \frac{x_0z_0}{2\sigma_{xz}^2}\right), \quad (20)$$

where x_0,z_0, and y_0 are the initial positions of an electron and $\sigma_{3\mathrm{D}}$ is the effective number of laser pulse periods the electron interacts with. The rms energy modulation waists are given by

$$\sigma_x \simeq \frac{\sqrt{w_{\rho_1}^2\omega_1^2 + w_{\rho_2}^2\omega_2^2}}{\sqrt{2}|\omega_1-\omega_2|}, \quad (21a)$$

$$\sigma_y = \frac{w_{\eta_1}w_{\eta_2}}{\sqrt{2}\sqrt{w_{\eta_1}^2 + w_{\eta_2}^2}}, \quad (21b)$$

$$\sigma_z \simeq \frac{c\sigma_{\varphi_1}\sigma_{\varphi_2}}{\sqrt{\sigma_{\varphi_1}^2\omega_1^2 + \sigma_{\varphi_2}^2\omega_2^2}}, \quad (21c)$$

and $\sigma_{xz} \to \infty$, where we assumed a relativistic electron beam $\gamma \gg 1$. The general expressions for arbitrary energy and geometry are given in Appendix D. The effective pulse length can be written as

$$\sigma_{3\mathrm{D}} = \frac{\sigma_\varphi}{\sqrt{1 + \left(\frac{c^2\gamma^2\sigma_\varphi^2}{\omega_1^2 w_{\rho 1}^2} + \frac{c^2\gamma^2\sigma_\varphi^2}{\omega_2^2 w_{\rho 2}^2}\right)\left[\beta^2 - \left(\frac{\omega_1-\omega_2}{\omega_1+\omega_2}\right)^2\right]}}, \quad (22)$$

which depends on the waist sizes w_{ρ_j} of the laser pulses in the propagation direction of the electron beam.

Equation (20) holds in the impulsive approximation when laser diffraction is negligible during the interaction. The latter condition is satisfied when the diffraction parameter $\psi \simeq w_\eta^2 w_\rho[\omega_1\omega_2/(w_\eta^4 + w_\rho^4)]^{1/2}/(c\gamma)$, with $w_\rho = w_{\rho_1} = w_{\rho_2}$ and $w_\eta = w_{\eta_1} = w_{\eta_2}$ satisfies the condition $\psi \ll 1$, see Appendix E. If the condition is not satisfied, the interaction length is shortened due to the finite Rayleigh lengths, resulting in a reduced effective interaction length given by $\sigma_{3\mathrm{D}} \to \sigma_{3\mathrm{D}}\sqrt{\pi}/\psi\,\mathrm{erfcx}(1/\psi)$, where $\mathrm{erfcx}(x) = \exp(x^2)[1 - 2/\sqrt{\pi}\int_0^x \exp(-y^2)dy]$ is the scaled complementary error function.

It is instructive to study the energy modulation amplitude [Eq. (20)] for a central electron with $(x_0, y_0, z_0) = (0,0,0)$ in the following three limits. First, in the limit where the waist size becomes very large such that $w_\rho = w_{\rho_1} = w_{\rho_2} \to \infty$, the plane wave case is retrieved where the effective pulse length $\sigma_{3\mathrm{D}} = \sigma_\varphi$. In this case, the modulation amplitude is correctly described by Eq. (6).

Second, for continuous wave lasers $\sigma_\varphi \to \infty$, the effective pulse length is given by $\sigma_{3\mathrm{D}} = \{\gamma^2c^2(\omega_1^{-2}w_{\rho_1}^{-2} + \omega_2^{-2}w_{\rho_2}^{-2})[\beta^2 - (\omega_1-\omega_2)^2/(\omega_1+\omega_2)^2]\}^{-1/2}$. In this limit,

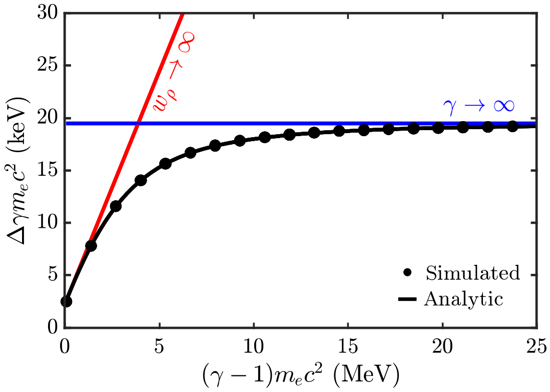

FIG. 8. Simulated (dots) and analytically calculated (black solid curve) energy modulation amplitude for $\sigma_\varphi = 50$, with $\sigma_{\varphi_1} = \sigma_{\varphi_2}$, $w_\rho = w_{\rho_1} = w_{\rho_2} = 50$ μm and $A_1 = A_2 = 0.01$.

the effective pulse length, and consequently the energy modulation, diverges when $\beta = (\omega_1 - \omega_2)/(\omega_1 + \omega_2)$, which is the case when the laser pulses are counterpropagating, see Eq. (5). In reality, however, the energy modulation will always be limited by laser diffraction, FEL interaction, or radial repulsion of the electron beam out of the laser beams.

Last, in the high energy limit, we find that the effective pulse length given by $\sigma_{3D} = \{\gamma^2 c^2(\omega_1^{-2} w_{\rho_1}^{-2} + \omega_2^{-2} w_{\rho_2}^{-2})[1-(\omega_1-\omega_2)^2/(\omega_1+\omega_2)^2]\}^{-1/2}$, which for equal waist sizes is given by $\sigma_{3D} = w_\rho/(2c\gamma)[\omega_1\omega_1(\omega_1+\omega_2)^2/(\omega_1^2+\omega_2^2)]^{1/2}$, is independent of the laser pulse length. This is caused by laser pulses nearly copropagating with the electron beam. Moreover, it scales inversely with the electron beam energy such that the energy modulation amplitude [Eq. (22)] becomes independent of beam energy. This is an important result since it gives the maximum energy modulation attainable by ponderomotive bunching using this geometry.

The results from the particle tracking simulation, shown in Fig. 8, confirm that Eq. (20) correctly describes the energy modulation. In the simulations TEM_{00}, Gaussian laser pulses were used. In the same figure, also the plane wave and high energy limit are given by the red and blue lines, respectively. The high energy limit can be extended by increasing both w_{ρ_j}. In practice, however, this also decreases the laser intensity for a given laser pulse energy since $A_1 A_2 \propto (w_{\rho_1} w_{\rho_2})^{-1/2}$. Therefore, the laser pulse energy determines the asymptotic energy modulation amplitude. In the simulation, the pulse energies are 0.3 and 0.95 mJ, respectively.

The optimal respective laser waists can be found by considering that the energy modulation scales as $\Delta\gamma \propto \sigma_{3D}(w_{\rho_1} w_{\rho_2})^{-1/2}$ for given laser pulse energies. By solving the differential equation $\partial\Delta\gamma/\partial w_{\rho 1} = 0$ for the laser waist $w_{\rho 1}$, we find that the optimum waist size is given by

$$w_{\rho_1}\Big|_{\max(\Delta\gamma)} = \frac{\omega_2 w_{\rho_2}}{\omega_1\sqrt{1 + \frac{\omega_2^2 w_{\rho_2}^2}{c^2\gamma^2\sigma_\varphi^2[\beta^2 - (\frac{\omega_1-\omega_2}{\omega_1+\omega_2})^2]}}} \tag{23}$$

which for relativistic electron beams ($\gamma \gg 1$) is written as $w_{\rho 1}|_{\max(\Delta\gamma)} \simeq \omega_2 w_{\rho 1}/\omega_1$. For the nominal set, the optimal waist leads to a relative increase in the energy modulation of about 30% with respect to the case of equal waist sizes. Note that the effective pulse length σ_{3D} is independent of the waists in laser polarization direction w_{η_j}. To attain maximum energy modulation with a constant laser pulse energy, it is possible to use a line focus, i.e., $w_{\eta_j} < w_{\rho_j}$, to increase the laser intensity during interaction. The smallest practicable line focus is limited by the electron beam waist and diffraction (see Appendix E).

To calculate the bunching factor, we consider a Gaussian distribution of monoenergetic electrons described by $f_0 = [(2\pi)^{3/2}\sigma_{e,x}\sigma_{e,y}\sigma_{e,z}]^{-1}\exp[-x_0^2/(2\sigma_{e,x}^2) - y_0^2/(2\sigma_{e,y}^2) - z_0^2/(2\sigma_{e,z}^2)]$, where $\sigma_{e,(x,y,z)}$ are the rms waists of the electron beam. Using the phase $\varphi = \varphi_0 + \zeta g(x_0, y_0, z_0)\sin\varphi_0$, with $g(x_0, y_0, z_0)$, the modulation envelope and $\zeta = L/f$ with $f = c\gamma^3\beta^3/[\Delta\gamma(\omega_1 - \omega_2)]$, the focal length of the center of the electron bunch with $\Delta\gamma$ the maximum energy modulation amplitude for an electron at the center of the bunch, we find that the bunching factor at $\kappa = n$ is given by $b(\kappa) = (-1)^n \int dx_0 dy_0 dz_0 f_0(x_0, y_0, z_0) J_n[n\zeta g(x_0, y_0, z_0)]$. This expression is the three-dimensional analog of Eq. (18). The integral can be evaluated if the Bessel function is represented by its power series $J_n(x) = \sum_{m=0}^{\infty} C_{m,n}(x/2)^{2m+n}$ with $C_{m,n} = (-1)^m/[m!(m+n)!]$, which reduces the three-dimensional integral to a single sum written as

$$b_n = b(n) = \sum_{m=0}^{\infty} \frac{(-1)^n C_{m,n}(\frac{1}{2}n\zeta)^{2m+n}}{\sqrt{\left(1 + \frac{(2m+n)\sigma_{e,y}^2}{\sigma_y^2}\right)\left[\left(1 + \frac{(2m+n)\sigma_{e,x}^2}{\sigma_x^2}\right)\left(1 + \frac{(2m+n)\sigma_{e,z}^2}{\sigma_z^2}\right) - \frac{(2m+n)^2\sigma_{e,x}^2\sigma_{e,z}^2}{4\sigma_{xz}^4}\right]}}. \tag{24}$$

This expression gives the bunching factor for a three-dimensional electron beam without emittance or energy spread with three-dimensional laser pulses without diffraction. The effects of energy spread and emittance can be included by taking into account the terms given in Eqs. (12) and (15), respectively. Note that these amendments

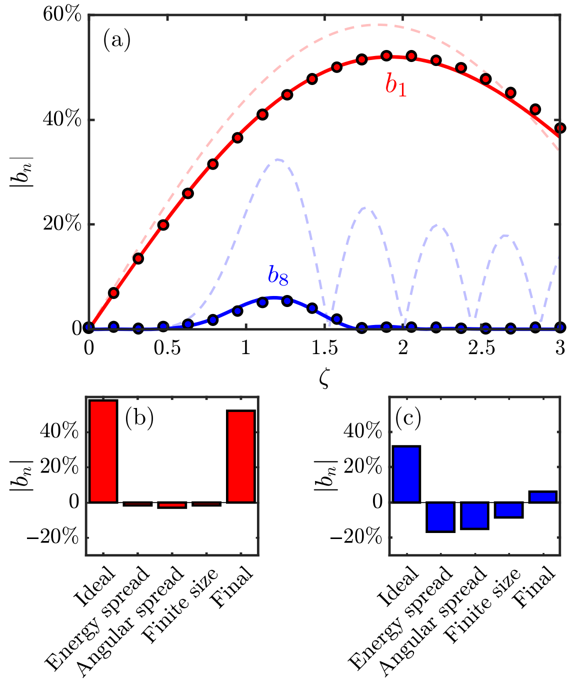

FIG. 9. (a) Simulated (dots) and analytically calculated (continuous curves) bunching factor including beam energy spread, angular spread, and finite beam size (parameters given in text). For reference, the plane wave case (dashed curves) is also shown. (b) and (c) Breakdown of bunching factor.

hold only by approximation since they do not explicitly take into account the energy modulation envelope.

In Fig. 9(a), the bunching factor is shown including all effects for a 4.6-MeV electron beam with $\sigma_\gamma = 10^{-3}$, $\sigma_\theta = 1$ mrad, $\sigma_{e,z} = 1$ μm, and $\sigma_{e,x} = \sigma_{e,y} = 5$ μm, and $\sigma_\varphi = 100$ laser pulses of 100 and 300 μJ, respectively, both focused to waists of 20 μm. The combination of Eqs. (12), (15), and (24) also are in good agreement with the particle tracking simulations. The bunching factor of the fundamental is close to the plane wave case, given by the dashed curve. The eighth harmonic, however is significantly affected: The maximum bunching factor of the eight harmonics is about $b_8 = 5\%$ at $\zeta = 1.2$, while it is 32% for the plane wave case. In Figs. 9(b) and 9(c), the separate effect (relative to the ideal case) of energy spread, angular spread, and finite size on the bunching factor is illustrated for the fundamental (b) and the eighth harmonic (c). From these figures, it is clear that the higher harmonic order is more significantly reduced by each effect.

V. PROPOSAL SUPERRADIANT EUV THOMSON SOURCE

To illustrate the practical use of the expressions derived in this paper, we will apply them to propose a superradiant extreme ultraviolet (EUV) ($\lambda = 13.6$ nm) Thomson source. We base the proposal on the beamline of Smartlight, which is an incoherent hard x-ray Thomson source that is currently being commissioned at the Eindhoven University of Technology [4]. The Thomson source will be driven by the advanced continuous-wave electron injector, which generates electron bunches up to 3 pC with ultralow normalized transverse emittance of 50 nm rad at a repetition rate of 1.5 GHz [26]. Downstream the electron gun is a high gradient X-band accelerator, based on a design for the compact linear collider at CERN, which accelerates bursts of 100 electron bunches to a beam energy between 6.4 MeV at 1-kHz repetition rate. Furthermore, we assume that the electron bunches exiting the accelerator have a FWHM bunch length of 50 fs with a relative rms energy spread of 10^{-4}.

We assume that the superradiant EUV Thomson source is driven by a long wave infrared (LWIR) laser which generates 1.5 ps pulses with a central wavelength of 10 μm, 1.5 ps pulse length, and 26 mJ at the same repetition rate as the electron bunches. The LWIR laser pulses are split into 25 mJ for Thomson scattering and 1 mJ for ponderomotive bunching. The second laser pulse used for the ponderomotive buncher has an ultraviolet (UV) central wavelength of 266 nm, 37 fs pulse length, and 100 μJ pulse energy. The modulation wavelength using these laser pulses is 272 nm.

To generate a beat wave resonant with the 6.4-MeV electron beam, the angles [Eq. (5)] with respect to the propagation axis of the electron beam are 457 and 11.7 mrad for the LWIR and UV laser pulse, respectively. We assume that for both the laser pulses, a line focus is applied with the following waist sizes: $w_{\rho_1} = 43$ μm, $w_{\rho_2} = \omega_2 w_{\rho_2}/\omega_1$, $w_{\eta_1} = 33$ μm, and $w_{\eta_2} = 0.55$ μm. This results in an effective beat wave pulse length $\sigma_{3D} = 45$, which is further reduced by about 63% by diffraction ($\psi = 1.38$). The short interaction length ensures that the phase drift during interaction is negligible.

The energy modulation amplitude [Eq. (20)] including diffraction in the proposed geometry is 35 keV resulting in a focal length [Eq. (7)] of about 1.5 mm. Considering the ratio of the initial electron beam energy spread and induced energy modulation we know from Eq. (12), there still should be significant bunching up to the 20th harmonic. The energy modulation waists, calculated using (21a)–(21c), are larger than the electron beam waist sizes, which in the transverse plane are taken to be $\sigma_{e,x} = \sigma_{e,y} = 3.6$ μm. The rms number of microbunches $N_b \simeq 20$. We find through Eq. (24) that the 20th harmonic is optimized around 1.8 mm after interaction with $b_{20} = 10\%$ bunching at a wavelength of 13.6 nm.

To generate EUV radiation, we consider a head-on scattering geometry with the laser pulse counterprogating the electron beam at an interaction angle of $\theta_0 = \pi$rad with respect to the propagating axis and pulse energy of $U_0 = 25$ mJ. A strong focus is applied to the Thomson laser beam with waists sizes $w_{\rho_0} = w_{\eta_0} = 20$ μm. Using this together with Eq. (8) and the efficiency factor that takes into account, the effect of the finite beam size ($\sigma_{e,x} = \sigma_{e,y} = 4.1$ μm at interaction), angular and energy spread on the superradiant yield into account, as given in [18], we calculate that the average superradiant power at the 20th harmonic is $P_{SR} = 1.6$ μW in 0.25% bandwidth assuming the laser pulses adhere to the 100-kHz repetition rate (in bursts). This is an increase of 862 with respect to the in-band incoherent emission. As a result of the smaller emission cone, the superradiant brightness is about 10^5 times higher than the incoherent brightness. Note that the total average power can be higher since, at this high order, neighboring harmonics might also contribute to the scattered radiation.

In terms of spectral power, this superradiant Thomson source compares to the best available high harmonic sources at the EUV wavelength [27]. To achieve an even higher average power, the X-band accelerator can be replaced by a superconducting accelerator operating at GHz repetition rate. In this case, the coherent flux is sufficient for advanced applications typically performed at FEL facilities such as ptychographic photomask inspection [28].

A method to achieve considerable bunching at higher order harmonics is by applying the energy modulation twice with a drift of many times the focal length in between. This has the advantage of requiring much lower energy modulation amplitude for a given energy spread to reach high order harmonics. At GeV electron beam energy, this so-called echo-enhanced modulation scheme [29] has been applied using magnetostatic modulators to achieve bunching at soft x-ray wavelengths [30]. Echo-induced ponderomotive bunching is beyond the scope of this paper but will be subject to future research.

VI. CONCLUSION

We have thoroughly analyzed the microbunching of an electron beam by two laser pulses at different frequencies and characterized the nonideal effects that are relevant to superradiant Thomson scattering experiments. The resulting expressions allow for fast (numerical) optimization of the electron beam phase space distribution to extremize the microbunching and, together with the expressions in [18], the yield of superradiant Thomson scattering. From our analysis, we find that using this method, significant bunching at EUV frequencies can be imposed on MeV electron beams. This results in a relative increase of $\sim 10^3$ in power and $\sim 10^5$ in brightness with respect to the incoherent mode. These findings can have a great impact on the development of compact powerful Thomson sources.

ACKNOWLEDGMENTS

This research was funded by the Ministry of Economic Affairs in the Netherlands through a TKI grant.

APPENDIX A: THE TIME-AVERAGED PONDEROMOTIVE FORCE

We use a pertubative approach where the four-velocity can be written as a $u^\mu = \sum_{j=0}^{\infty} u_j^\mu$, where $u_n^\mu \propto A^n$ with vector potential amplitude satisfying the condition $A < 1$ to evaluate the Lorentz force equation

$$\partial_{c\tau}(u^\mu - A^\mu) = -u_\nu \partial^\mu A^\nu \tag{A1}$$

up to the second order. Assuming that the propagation direction of the electrons is normal to the laser polarization direction such that $\epsilon_\nu u_0^\nu = 0$, ensures that the right-hand side of Eq. (A1) is equal to zero. In this case the first order four-velocity is $u_1^\mu = A^\mu$, which is substituted into (A1) to find the second order four-velocity

$$\partial_{c\tau} u_2^\mu = -\frac{1}{2} \partial^\mu A_\nu A^\nu. \tag{A2}$$

Using the plane wave four-potential Eq. (1), the contraction can be written as

$$\begin{aligned} A_\nu A^\nu = -\frac{1}{2}(A_1^2 + A_2^2 + A_1^2 \cos 2\varphi_1 + A_2^2 \cos 2\varphi_2) \\ - A_1 A_2 \cos\varphi_+ - A_1 A_2 \cos\varphi_-, \end{aligned} \tag{A3}$$

where $\varphi_\pm = \varphi_1 \pm \varphi_2$. Averaging over the fast time scales leads to the ponderomotive potential [Eq. (3)]. The four-velocity $u^\mu \simeq u_0^\mu + u_1^\mu + u_2^\mu$ averaged over the fast time scales is given by $\bar{u}^\mu = u_0^\mu + u_2^\mu$. Note that Eq. (A3) also holds for varying four-potential amplitude.

APPENDIX B: IMPULSIVE APPROXIMATION

The ponderomotive force [Eq. (2)] with the ponderomotive potential (3) can be rewritten to a second order pendulum equation by taking the contraction with k_-^μ on both sides:

$$\partial_{c\tau}^2 \varphi_- + \frac{1}{2} A_1 A_2 k_-^\nu k_{-\nu} \sin\varphi_- = 0, \tag{B1}$$

where we used $k_-^\nu \bar{u}_\nu = \partial_{c\tau}\varphi_-$. This is a laser pulse based analog to the familiar pendulum equation for low-gain FEL [31]. It is straightforward to show that for small ponderomotive phases $\varphi_- \ll 1$, a solution to the pendulum equation for a resonant electron is given by $\varphi_- = \varphi_0 \cos\Omega\tau$, where the oscillation frequency is given by $\Omega = c(A_1 A_2 k_-^\nu k_{-\nu}/2)^{1/2}$. The phase drift of a resonant electron is negligible when the interaction proper time τ_0 satisfies the following condition:

$$\tau_0 \ll \frac{2\pi}{\Omega} = \frac{2\sqrt{2}\pi}{c\sqrt{A_1 A_2 k_-^\nu k_{-\nu}}}. \tag{B2}$$

If this condition holds, we can write the four-position of the electron during interaction as the ballistic motion before interaction $x^\mu \simeq x_0^\mu + u_0^\mu c\tau$, which we refer to as the impulsive approximation.

APPENDIX C: BUNCH TILT

The ponderomotive bunching method also allows for the generation of bunches with a tilt angle in one of the transverse planes as shown in Fig. 10. In a FEL, such tilted microbunches have led to the generation of strong off-axis radiation [32]. Conversely, in an oblique Thomson scattering geometry, a tilt angle is highly relevant since it could direct the superradiance back on-axis, permitting the use of higher electron beam energy which may result in an increase of yield by orders of magnitude [18].

To produce a tilted density modulation, the ponderomotive beat wave and consequently the four-velocity modulation, given by Eq. (4), should have a nonzero component in the x direction. The ratio between the transverse and longitudinal momentum modulation determines tilt angle α such that $\tan\alpha = k_-^{(1)}/k_-^{(3)}$. Also in this case, the resonance condition $k_-^{\nu}u_{0\nu} = 0$ requires that the longitudinal component of the beat wave four-vector $k_-^{(3)} = \omega_1/c\,\cos\theta_1 - \omega_2/c\,\cos\theta_2 = (\omega_1-\omega_2)/(c\beta)$ remains the same as for nontilted microbunching since the beat wave should propagate at the same velocity as the electron beam for optimal energy modulation. By substituting $k_-^{(3)}$ in the expression for the tilt angle, we find that the transverse component is given by $k_-^{(1)} = \omega_1/c\,\sin\theta_1 - \omega_2/c\,\sin\theta_2 = (\omega_1-\omega_2)\tan\alpha/(c\beta)$. These two conditions generalize the laser beam angles at which resonance is attained given by Eq. (5) to include the tilt angle. For a relativistic electron beam, these angles are given by

$$\cos\theta_1 = \frac{\cos^2\alpha}{\beta}\left[1 - \frac{1}{2\gamma^2}\frac{\omega_1+\omega_2}{\omega_1} + \frac{\omega_1-\omega_2}{2\omega_1}\tan^2\alpha\right] \mp \frac{|\omega_1-\omega_2|}{\beta\omega_1}\frac{X}{2\gamma^2}, \tag{C1}$$

where $X = \{\tan^2\alpha(1-\beta^2\cos^2\alpha)[\beta^2\cos^2\alpha(\omega_1+\omega_2)^2/(\omega_1-\omega_2)^2-1]\}^{1/2}$. The angle θ_2 can be found by changing the subscripts in (C1) from $1\to2$ and vice versa. For finite bunch tilt angle, there are two pairs of possible laser beam angles that produce a resonant beat wave, which produces the correct bunch tilt depending on the respective sign of the laser beam angles. When the laser beam angles θ_j have the same (opposite) sign the minus (plus) sign is correct. The interaction time is shorter for laser incidence angles with opposite sign, resulting in a lower energy modulation amplitude. Note that Eq. (C1) reduces to Eq. (5) for a tilt angle of zero.

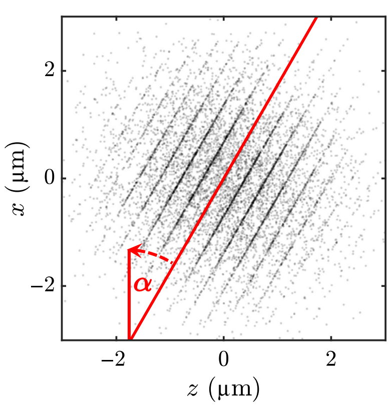

FIG. 10. Simulated electron bunch with microbunch tilt.

The bunching tilt that can be imposed using this method is determined by the laser frequencies. The largest tilt angle attainable is $\alpha_{\max} = \arccos[(\omega_1-\omega_2)/(\omega_1+\omega_2)/\beta]$. For larger tilt angles, the parameter X, and subsequently the laser beam angles described by Eq. (C1), become complex. In principle, large tilt angles near 90° can be induced by using laser pulses with central frequencies that are close to each other. However, this limits the energy modulation amplitude and the modulation frequency significantly. For the nominal set of parameters, the maximum tilt angle is 60°.

For relativistic electron beams, the modulation of the transverse velocity is much larger than the modulation in axial velocity. As a consequence, the focal length for large tilt angles can be considerably reduced with respect to longitudinal modulation. This becomes clear from the phase after energy modulation, which for nonzero tilt angle is given by $\varphi = k_-^{\nu}(u_{0\nu}+\Delta u_{\nu}) = \varphi_0 + L\Delta\gamma/(\gamma^3\beta^2)(1+\gamma^2\tan^2\alpha)\sin\varphi_0$. Expanding the phase around $\varphi_0 = \pi$ and setting it to zero gives the focal length

$$f = \frac{c\gamma^3\beta^3}{\Delta\gamma(1+\gamma^2\tan^2\alpha)}\frac{1}{\omega_1-\omega_2}. \tag{C2}$$

For the same energy modulation amplitude as the nominal set, the focal length for the maximum tilt angle is 66 μm, several orders of magnitude shorter than the longitudinal modulation focal length. However, note that more pulse energy is required to attain an energy modulation in a geometry that induces microbunch tilt since the laser angles of incidence change are larger.

APPENDIX D: MODULATION ENVELOPE

The ponderomotive force equation for three-dimensional laser pulses has the following form:

$$\partial_{c\tau}\bar{u}^{\mu} = -\frac{1}{2}A_1A_2\exp\left(-W^{\mu\nu}x_{\mu}x_{\nu}\right)\sin\left(k_-^{\nu}x_{\nu}\right)k_-^{\mu}, \tag{D1}$$

where $W^{\mu\nu} = (r_1^{\mu}r_1^{\nu}+r_2^{\mu}r_2^{\nu})/w_{\rho}^2 + 2\epsilon^{\mu}\epsilon^{\nu}/w_{\eta}^2 + k_1^{\mu}k_1^{\nu}/(2\sigma_{\varphi_1}^2) + (k_2^{\mu}k_2^{\nu})/(2\sigma_{\varphi_2}^2)$. By imposing the impulsive approximation $x^{\mu} \simeq x_0^{\mu} + u_0^{\mu}c\tau$, where u_0^{μ} is considered on-resonance such that $k_-^{\nu}x_{\nu} \simeq \varphi_0$, we can identify that the argument of the exponent can be written as a second order polynomial in τ given by $W^{\mu\nu}x_{\mu}x_{\nu} \simeq c_2\tau^2 + c_1\tau + c_0$, where $c_0 = W^{\mu\nu}x_{0\mu}x_{0\mu}$, $c_1 = 2W^{\mu\nu}cu_{0\nu}x_{0\mu}$, and $c_2 = W^{\mu\nu}c^2u_{0\nu}u_{0\mu}$. Here $\tau_{3D} = 1/\sqrt{c_2}$ is the eigen interaction time on an electron with the beat wave. Substituting the polynomial into Eq. (D1) and integrating using the standard integral $\int_{-\infty}^{\infty}\exp(-c_2x^2-c_1x-c_0)dx=\sqrt{\pi/c_2}\exp[c_1^2/(4c_2)-c_0]$ results in the modulation four-velocity

$$\Delta u^\mu = \sqrt{\pi}A_1A_2c\tau_{3\mathrm{D}}\ \exp\left(-W^{\mu\nu}_{\mathrm{mod}}x_{0\mu}x_{0\nu}\right)\sin\varphi_0k^\mu_-, \tag{D2}$$

where the modulation amplitude tensor is given by

$$W^{\mu\nu}_{\mathrm{mod}} = W^{\mu\nu} - \frac{W^{\mu\kappa}W^{\nu\lambda}u_{0\kappa}u_{0\lambda}}{W^{\alpha\beta}u_{0\alpha}u_{0\beta}} \tag{D3}$$

which for the geometry discussed in this paper and $x_0^0=0$ reduces to the form found in Eq. (20).

APPENDIX E: LASER BEAM DIFFRACTION

In Sec. IV, we considered the interaction to take place near the waist of the laser pulses. For tightly focused lasers (e.g., with a line focus), however, diffraction might adversely affect the bunching process by the reduced interaction time as a result of decreasing laser intensity or by electrons probing different phases of the beat wave due to the nonplanar wavefronts. Here, we will approximate the effect of diffraction by only taking into account the reduction of laser intensity.

The reduction of the four-potential amplitude due to diffraction is considered by making the substitution $A_j\to A_j/g_j$ in Eq. (19), where

$$g_j = (1+\zeta_j^2/z^2_{R\rho_j})^{1/4}(1+\zeta_j^2/z^2_{R\eta_j})^{1/4}. \tag{E1}$$

Here, $\zeta_j = s_j^\nu x_\nu$ is the longitudinal laser coordinate with $s_j^\mu = (0,-\sin\theta_j\mathbf{e}_x+\cos\theta_j\mathbf{e}_z)$, a four-vector denoting the longitudinal direction of the jth laser pulse, and $z_{R\rho_j}=\omega_jw^2_{\rho_j}/(2c)$ and $z_{R\eta_j}=\omega_jw^2_{\eta_j}/(2c)$ the Rayleigh lengths of jth laser pulse corresponding to the mutually orthogonal transverse directions.

To find an analytical solution to the resulting equation of motion, we have to make the following two approximations. First, we impose the impulsive approximation for a resonant central electron such that $x^\mu\simeq u_0^\mu c\tau$. Second, the resulting product of the diffraction terms g_1g_2 should be expanded to second order in τ such that

$$g_1g_2\simeq 1+\tau^2/\tau_R^2, \tag{E2}$$

where

$$\tau_R = \frac{2\gamma}{c^2}\left[\frac{(\omega_1+\omega_2-2\gamma^2\omega_1)^2}{\omega_1^4}\left(\frac{1}{w^4_{\rho_1}}+\frac{1}{w^4_{\eta_1}}\right) + \frac{(\omega_1+\omega_2-2\gamma^2\omega_2)^2}{\omega_2^4}\left(\frac{1}{w^4_{\rho_2}}+\frac{1}{w^4_{\eta_2}}\right)\right]^{-1/2} \tag{E3}$$

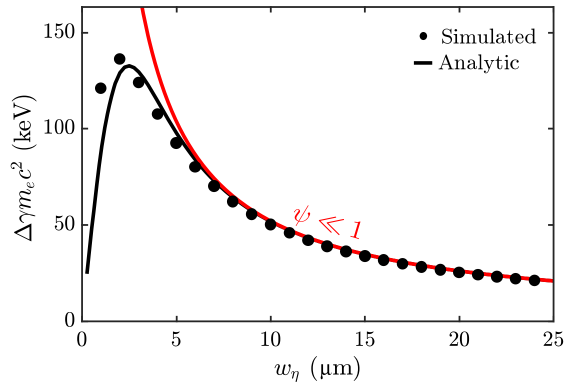

FIG. 11. Simulated (dots) and analytical (curves) electron energy modulation for a varying laser waist with (black curve) and without diffraction (red curve). The normalized pulse length of both lasers is $\sigma_\varphi = 50$.

is the approximated proper interaction time of a central electron with the ponderomotive beat wave due to diffraction only. Integration over proper time leads to the following energy modulation:

$$\Delta\gamma = \pi A_1A_2\gamma\sigma_{3\mathrm{D}}\frac{\omega_1-\omega_2}{\omega_1+\omega_2}\frac{\mathrm{erfcx}(\psi^{-1})}{\psi}, \tag{E4}$$

where $\mathrm{erfcx}(x)=\exp(x^2)[1-2/\sqrt{\pi}\int_0^x\exp(-y^2)dy]$ is the scaled complementary error function and diffraction parameter ψ is the interaction time scaled by the interaction time due to diffraction only:

$$\psi = \frac{2\sigma_{3\mathrm{D}}\gamma}{(\omega_1+\omega_2)\tau_R}. \tag{E5}$$

When $\psi\ll 1$, the effect of diffraction is negligible and Eq. (E4) condenses to Eq. (20) (with $x_0^\mu=0$). On the other hand, when $\psi\gg 1$, diffraction dominates such that the diffraction term can be approximated by $\mathrm{erfcx}(\psi^{-1})/\psi\simeq 1/\psi$.

In Fig. 11, the results of particle tracking simulations show that Eq. (E4) describes the energy modulation reasonably well. In the simulations, a line focus was applied for the nominal set and Gaussian laser pulses with fixed energy (both 0.3 mJ). To this end, the waists $w_\rho = w_{\rho_1}=w_{\rho_2}=15$ μm is kept constant (for a constant interaction time without diffraction) and $w_\eta = w_{\eta_1}=w_{\eta_2}$ is varied. The maximum energy modulation amplitude is found around $w_\eta = 2.5$ μm. However, this might not be the optimal setting for microbunching when taking into account the finite transverse waist of the electron beam.

[1] Y. Du, L. Yan, J. Hua, Q. Du, Z. Zhang, R. Li, H. Qian, W. Huang, H. Chen, and C. Tang, Rev. Sci. Instrum. 84, 053301 (2013).

[2] A. Bacci *et al.*, in *Proceedings of the International Particle Accelerator Conference* (JACoW, Geneva, Switzerland, 2014), pp. 2238–2241.

[3] E. Eggl, M. Dierolf, K. Achterhold, C. Jud, B. Günther, E. Braig, B. Gleich, and F. Pfeiffer, J. Synchrotron Radiat. **23**, 1137 (2016).

[4] X. F. D. Stragier, P. H. A. Mutsaers, and O. J. Luiten, Microsc. Microanal. **24**, 310 (2018).

[5] K. Dupraz *et al.*, Phys. Open **5**, 100051 (2020).

[6] W. S. Graves, F. X. Kärtner, D. E. Moncton, and P. Piot, Phys. Rev. Lett. **108**, 263904 (2012).

[7] E. A. Nanni, W. S. Graves, and D. E. Moncton, Phys. Rev. Accel. Beams **21**, 014401 (2018).

[8] D. C. Nguyen and B. E. Carlsten, Nucl. Instrum. Methods Phys. Res., Sect. A **375**, 597 (1996).

[9] M. Boscolo, M. Ferrario, I. Boscolo, F. Castelli, and S. Cialdi, Nucl. Instrum. Methods Phys. Res., Sect. A **577**, 409 (2007).

[10] A. J. McCulloch, D. V. Sheludko, S. D. Saliba, S. C. Bell, M. Junker, K. A. Nugent, and R. E. Scholten, Nat. Phys. **7**, 785 (2011).

[11] A. J. McCulloch, D. V. Sheludko, M. Junker, and R. E. Scholten, Nat. Commun. **4**, 1692 (2013).

[12] K. E. Priebe, C. Rathje, S. V. Yalunin, T. Hohage, A. Feist, S. Schäfer, and C. Ropers, Nat. Photonics **11**, 793 (2017).

[13] M. Kozák, J. McNeur, K. J. Leedle, H. Deng, N. Schönenberger, A. Ruehl, I. Hartl, J. S. Harris, R. L. Byer, and P. Hommelhoff, Nat. Commun. **8**, 14342 (2017).

[14] N. Schönenberger, A. Mittelbach, P. Yousefi, J. McNeur, U. Niedermayer, and P. Hommelhoff, Phys. Rev. Lett. **123**, 264803 (2019).

[15] J. T. Moody, R. K. Li, P. Musumeci, C. M. Scoby, and H. To, AIP Conf. Proc. **1507**, 722 (2012).

[16] M. Kozák, T. Eckstein, N. Schönenberger, and P. Hommelhoff, Nat. Phys. **14**, 121 (2018).

[17] M. Kozák, N. Schönenberger, and P. Hommelhoff, Phys. Rev. Lett. **120**, 103203 (2018).

[18] B. H. Schaap, T. D. C. d. Vos, P. W. Smorenburg, and O. J. Luiten, New J. Phys. **24**, 033040 (2022).

[19] Pulsar Physics, General Particle Tracer (GPT), http://www.pulsar.nl/gpt.

[20] L. H. Yu, Phys. Rev. A **44**, 5178 (1991).

[21] T. Van Oudheusden, E. F. De Jong, S. B. Van Der Geer, W. P. Op 'T Root, O. J. Luiten, and B. J. Siwick, J. Appl. Phys. **102**, 093501 (2007).

[22] J. Maxson, D. Cesar, G. Calmasini, A. Ody, P. Musumeci, and D. Alesini, Phys. Rev. Lett. **118**, 154802 (2017).

[23] W. F. Toonen, X. F. Stragier, P. H. Mutsaers, and O. J. Luiten, Phys. Rev. Accel. Beams **22**, 123401 (2019).

[24] A. Bartnik, C. Gulliford, I. Bazarov, L. Cultera, and B. Dunham, Phys. Rev. ST Accel. Beams **18**, 083401 (2015).

[25] F. Sannibale, D. Filippetto, H. Qian, C. Mitchell, F. Zhou, T. Vecchione, R. K. Li, S. Gierman, and J. Schmerge, Rev. Sci. Instrum. **90**, 033304 (2019).

[26] W. F. Toonen, A. Rajabi, R. G. van den Berg, X. F. Stragier, P. H. Mutsaers, P. W. Smorenburg, and O. J. Luiten, Nucl. Instrum. Methods Phys. Res., Sect. A **1013**, 165678 (2021).

[27] L. Loetgering, S. Witte, and J. Rothhardt, Opt. Express **30**, 4133 (2022).

[28] I. Mochi, S. Fernandez, R. Nebling, U. Locans, R. Rajeev, A. Dejkameh, D. Kazazis, L.-T. Tseng, S. Danylyuk, L. Juschkin, and Y. Ekinci, J. Micro/ Nanolithogr. MEMS MOEMS **19**, 014002 (2020).

[29] G. Stupakov, Phys. Rev. Lett. **102**, 074801 (2009).

[30] P. R. Ribič *et al.*, Nat. Photonics **13**, 555 (2019).

[31] P. Schmüser, M. Dohlus, J. Rossbach, and C. Behrens, *Free-Electron Lasers in the Ultraviolet and X-Ray Regime*, 2nd ed. (Springer, Cham, 2014), https://doi.org/10.1007/978-3-319-04081-3.

[32] J. P. Macarthur, A. A. Lutman, J. Krzywinski, and Z. Huang, Phys. Rev. X **8**, 041036 (2018).